Journal of Experimental and Theoretical Physics, Vol. 91, No. 4, 2000, pp. 801–816.
From Zhurnal Éksperimental'noĭ i Teoreticheskoĭ Fiziki, Vol. 118, No. 4, 2000, pp. 923–940.

SOLIDS
Electronic Properties

Phenomenological Description of the Microwave Surface Impedance and Complex Conductivity of High-T_c Single Crystals¶

M. R. Trunin[a, *], Yu. A. Nefyodov[a], and H. J. Fink[b]

[a]*Institute of Solid-State Physics, Russian Academy of Sciences, Chernogolovka, Moscow oblast, 142432 Russia*
**e-mail: trunin@issp.ac.ru*

[b]*Department of Electrical and Computer Engineering, University of California, Davis, California 95616, USA*

Received May 4, 2000

Abstract—Measurements of the microwave surface impedance $Z_s(T) = R_s(T) + iX_s(T)$ and the complex conductivity $\sigma_s(T)$ in the *ab*-plane of high-quality high-T_c YBCO, BSCCO, TBCCO, and TBCO single crystals are analyzed. Experimental data of $Z_s(T)$ and $\sigma_s(T)$ are compared with calculations based on a modified two-fluid model that includes a temperature-dependent quasiparticle scattering and a unique temperature variation of the density of superconducting carriers. We describe the agreement and disagreement of our analysis with the salient features of the experimental data. We review the existing microscopic models based on unconventional symmetry types of the order parameter and on novel quasiparticle relaxation mechanisms. © *2000 MAIK "Nauka/Interperiodica".*

1. INTRODUCTION

High-precision microwave measurements of the temperature dependence of the surface impedance $Z_s(T) = R_s(T) + iX_s(T)$ of high-T_c superconductors (HTSC's) considerably advance our understanding about the pairing of the superconducting electrons in these materials. In particular, in 1993, the linear *T*-dependence of the penetration depth $\lambda(T) - \lambda(0) \propto \Delta X_s(T) \propto T$ observed below 25 K in the *ab*-plane of high-quality $YBa_2Cu_3O_{6.95}$ (YBCO) single crystals [1] gave rise to productive investigations of the order parameter of HTSC's. This linear variation of $\lambda(T)$ at low *T* has by now been observed not only in orthorhombic YBCO single crystals [2–14] and films [15–18] but also in tetragonal $Bi_2Sr_2CaCu_2O_8$ (BSCCO) [19–22], $Tl_2Ba_2CuO_{6+\delta}$ (TBCO) [23, 24], and $Tl_2Ba_2CaCu_2O_{8-\delta}$ (TBCCO) [10] single crystals. This temperature dependence does not agree with the nearly isotropic superconducting gap, and it is now considered as a strong evidence for the *d*-wave pairing in these materials [25–35] in spite of the fact that the experimental data are not sensitive to the phase of the superconducting order parameter. Later research has shown that $\Delta\lambda_{ab}(T)$ can be linear at low *T* for models invoking the proximity effect between normal and superconducting layers [36] or assuming the anisotropic *s*-wave pairing [37–39]. However, none of these theories can give an explanation for the substantially different slopes of $\Delta\lambda_{ab}(T)$ at low *T* in the YBCO samples grown by different methods [40] and for certain features such as a bump [9, 11, 16, 41] or a plateau [8, 10, 12], which are observed in the intermediate temperature range $0.4\,T_c < T < 0.8\,T_c$. Models containing a mixed $(d + s)$ symmetry of the order parameter [42–56] hold some promise for a successful description of these experimental features, but this would require additional theoretical investigations.

Another important feature of the microwave response of HTSC crystals is the linear variation with temperature of the surface resistance $R_s(T)$ in the *ab*-plane at low temperatures. At frequencies about 10 GHz and below, the *T*-dependence of $R_s(T)$ in BSCCO, TBCO, and TBCCO single crystals is linear over the range $0 < T \lesssim T_c/2$ [19, 21–23]. For YBCO crystals, $\Delta R_s(T) \propto T$ for $T \lesssim T_c/3$ and $R_s(T)$ displays a broad peak with a valley at higher temperatures [4–14, 57–61]. This peak can be understood as a competition between an increase in the quasiparticle lifetime and a decrease in the quasiparticle density as the temperature is lowered. The sufficiently slow decrease in the quasiparticle density is indicative of a highly anisotropic or unconventional order parameter, resulting in a very small or vanishing energy gap, while the increase in the quasiparticle lifetime is attributed to the presence of inelastic scattering, which can be due (i) to the exchange of antiferromagnetic spin fluctuations [62], which would naturally lead to the *d*-wave pairing, or (ii) to a strong electron–phonon interaction [63–65] within the anisotropic *s*-wave pairing model [66, 67]. Moreover, there have been suggestions of unconventional states for describing the charge carriers in

¶ This article was submitted by the authors in English.

the CuO_2 planes like the marginal Fermi liquid [68, 69] and the Luttinger liquid [70, 71]. However, to fit the data of YBCO, the inelastic scattering rate must decrease with temperature much faster than predicted by any of these microscopic models. Further, the *d*-wave model with point scatterers does predict a finite low-temperature and low-frequency limit, which is independent of the concentration and the strength of the scattering centers [72]. Therefore, the latter model does not explain the very different values of the observed residual surface resistance $R_{res} \equiv R_s$ ($T \longrightarrow 0$) on different samples. Furthermore, the value of this universal surface resistance is much lower than the R_{res}values obtained from experiments. There is no microscopic theory explaining the linear temperature dependence of $\Delta R_s(T)$ up to $T_c/2$ in crystals with a nonorthorhombic structure and the shoulder of $R_s(T)$observed on YBCO [9, 11] for $T > 40$ K.

In the absence of a generally accepted microscopic theory, a modified two-fluid model for calculating $Z_s(T)$ in HTSC single crystals has been proposed independently in [73, 74] and then further developed in [8, 40, 61, 75]. Our phenomenological model has two essential features that make it different from the well-known Gorter–Casimir model [76]. The first is the introduction of the temperature dependence of the quasiparticle relaxation time $\tau(t)$ (with $t \equiv T/T_c$) described by the Gruneisen formula (electron-phonon interaction), and the second feature is the unique density of superconducting electrons $n_s(t)$, which gives rise to a linear temperature dependence of the penetration depth in the *ab*-plane at low temperatures:

$$\frac{\lambda^2(0)}{\lambda^2(t)} = \frac{n_s(t)}{n} \simeq 1 - \alpha t, \tag{1}$$

where $n = n_s + n_n$ is the total carrier density and α is a numerical parameter in our model.

The goal of this paper is to demonstrate the power of our model in describing the general and distinctive features of the surface impedance $Z_s(T)$ and the complex conductivity $\sigma_s(T)$ in the superconducting and normal states of different HTSC crystals (whose doping level corresponds to the highest T_c) at various frequencies. Section 2 describes the systematization of the $Z_s(T)$ measurements, including the analysis that is used to extract $\sigma_s(T)$ from the measured values of $Z_s(T)$. Section 3 compares experimental data of $Z_s(T)$ and $\sigma_s(T)$ over the entire temperature range with calculations based on our modified two-fluid model. In the conclusion, we compare the concepts of our model with results of microscopic theories. We hope that this can be a helpful guide for future investigations of microwave properties of HTSC's from a microscopic point of view.

2. ANALYSIS OF EXPERIMENTAL RESULTS

2.1. Surface Impedance

The surface impedance in the *ab*-plane of HTSC's, expressed in terms of the complex conductivity $\sigma_s = \sigma_1 - i\sigma_2$, obeys the local equation

$$Z_s = R_s + iX_s\left(\frac{i\omega\mu_0}{\sigma_1 - i\sigma_2}\right)^{1/2}. \tag{2}$$

The impedance components are

$$R_s = \sqrt{\frac{\omega\mu_0(\varphi^{1/2} - 1)}{2\sigma_2\varphi}}, \tag{3}$$

$$X_s = \sqrt{\frac{\omega\mu_0(\varphi^{1/2} + 1)}{2\sigma_2\varphi}}, \tag{4}$$

where $\varphi = 1 + (\sigma_1/\sigma_2)^2$. It is obvious that $R_s < X_s$ for $T < T_c$.

For temperature $T < T_c$ and with $\sigma_1 \ll \sigma_2$, Eqs. (3) and (4) reduce to

$$R_s \simeq \frac{(\omega\mu_0)^{1/2}\sigma_1}{2\sigma_2^{3/2}} = \frac{1}{2}\omega^2\mu_0^2\sigma_1\lambda^3, \qquad X_s \simeq (\omega\mu_0/\sigma_2)^{1/2} = \omega\mu_0\lambda. \tag{5}$$

The surface impedance components are measurable quantities. The real part of the surface impedance, the surface resistance R_s, is proportional to the loss of the microwave power. It is caused by the presence of "normal" carriers. In the centimeter wavelength band, typical values of the surface resistance in the *ab*-plane of HTSC single crystals are between 0.1 and 0.3 Ω above the transition temperature T_c. When T is decreased through T_c, the surface resistance abruptly drops but does not seem to approach zero as $T \longrightarrow 0$. In conventional superconductors (like Nb), $R_s(T)$ decreases exponentially upon decreasing the temperature below $T_c/2$, approaching a constant residual surface resistance R_{res} as $T \longrightarrow 0$. R_{res} is due to the presence of various defects in the surface layer of the superconductor. Therefore, it is generally accepted that lowering R_{res} leads to improving the sample quality. In high-quality HTSC's, there is no plateau in $R_s(T)$ for $T \ll T_c$. However, we extrapolate the value of $R_s(T)$ to $T = 0$ K and denote it by R_{res}. The origin of the residual surface resistance observed in HTSC crystals remains unclear. It is known that R_{res} is strongly material and sample dependent and is approximately proportional to the square of the frequency. At present, very small values ($R_{res} \approx 20$ $\mu\Omega$ at frequencies $\approx$10 GHz) are observed in YBCO single crystals [9, 14].

The imaginary part of the surface impedance, the reactance X_s, is mainly determined by the superconducting carriers and is due to nondissipative energy stored in the surface layer of the superconductor.

In the table, we summarize the main features of the temperature dependence of the surface impedance of high-quality YBCO, BSCCO, TBCO, and TBCCO single crystals whose residual surface resistance in the *ab*-plane (R_{res}) is less than one milliohm at the frequency ≈10 GHz with the $R_s(T_c)$ values about 0.1 Ω. There is good reason to believe that the temperature behavior of the electrodynamic parameters of these crystals is adequately related to the intrinsic microscopic properties of the superconducting state of HTSC.

To illustrate the data of the table, we show in Fig. 1, as an example, experimental data of $R_s(T)$ and $X_s(T)$ in the *ab*-plane of a BSCCO single crystal at 9.4 GHz [22]. In this figure, $R_s(T) = X_s(T)$ for $T \geq T_c$, which corresponds to the normal skin-effect condition. Knowing $R_s(T_c) = \sqrt{\omega\mu_0\rho(T_c)/2} \approx 0.12$ Ω, we obtain the resistivity $\rho(T_c) \approx 40$ μΩ cm. In the normal state (above T_c), the temperature dependence of $R_s(T) = X_s(T)$ is adequately described by the expression $2R_s^2(T)/\omega\mu_0 = \rho(T) = \rho_0 + bT$. For the BSCCO crystal in Fig. 1, $\rho_0 \approx 13$ μΩ cm and $b \approx 0.3$ μΩ cm/K. The insets in Fig. 1 show $R_s(T)$ and $\lambda(T) = X_s(T)/\omega\mu_0$ for $T < 0.7\ T_c$ plotted on a linear scale. The extrapolation of the low-temperature sections of these curves to $T = 0$ K yields the estimates $R_{res} \approx 0.5$ mΩ and $\lambda_{ab}(0) = 2600$ Å for this crystal.

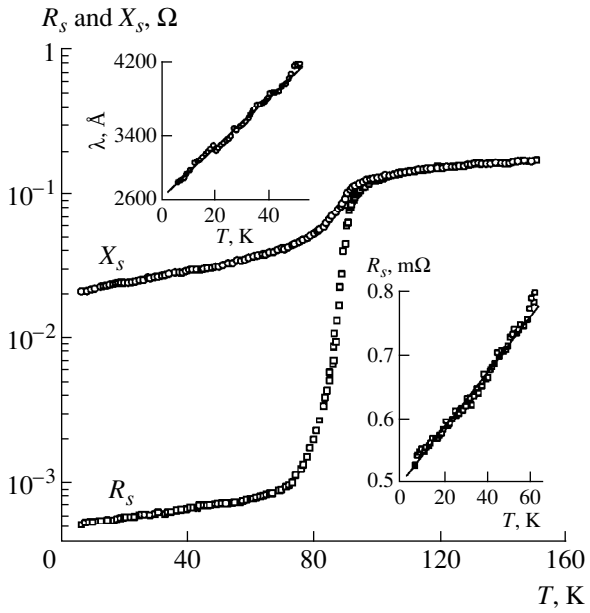

Fig. 1. Surface resistance $R_s(T)$ and reactance $X_s(T)$ in the *ab*-plane of a BSCCO single crystal at 9.4 GHz. The insets show linear plots of $\lambda(T)$ and $R_s(T)$ at low temperatures.

The experimental curves of $\Delta\lambda_{ab}(T)$ for YBCO, TBCO, and TBCCO crystals are also linear in the range $T < T_c/3$. It is important to note different slopes of the $\Delta\lambda(T) \propto T$ curves for $T \ll T_c$. In particular, in YBCO crystals fabricated by different techniques, the slopes of $\Delta\lambda_{ab}(T)$ differ by almost one order of magnitude [8, 9, 13]. The reasons for such a discrepancy are still unclear.

At frequencies about 10 GHz and below, the linear dependence $\Delta R_s(T) \propto T$ in BSCCO (Fig. 1), TBCCO, and TBCO single crystals may actually extend to the temperatures $\sim T_c/2$. This property, which is common for all HTSC crystals with the tetragonal structure, is not characteristic of YBCO. As noted previously, all microwave measurements on high-quality YBCO single crystals show a broad peak in the $R_s(T)$ curve centered near 30–40 K up to the frequencies ≈10 GHz. The peak shifts to higher temperatures and diminishes in size as the frequency is increased. In higher quality YBCO crystals, the peak amplitude increases and $R_s(T)$ reaches its maximum at a lower temperature [14].

The underlying origin of this YBCO feature has remained unclear. The simplest idea is that the absence of this peak in crystals with tetragonal structure might be caused by their "poor" quality, as is the case with YBCO doped with Zn [2, 4, 58]. However, this conclusion is probably incorrect because (i) there is a sufficiently large set of experimental data indicating that $R_s(T)$ is a linear function of T for BSCCO, TBCO, and TBCCO, and (ii) the peak in $R_s(T)$ was also detected in the YBCO crystals [7, 10, 60] with the parameters R_{res} and $\rho(T_c)$ that would characterize the quality of these crystal as being "poor" compared to those of, for example, TBCCO [10] or BSCCO [21]. Results for the latter crystals are shown in Fig. 2. The more probable cause of the peak, however, is the presence of an additional component in the YBCO orthorhombic structure, namely, the CuO chains that lead to a mixed ($d + s$) symmetry of the order parameter in YBCO. The electrons of the chains form an additional band, contributing to the observed *T*-dependence of $Z_s(T)$. This contribution seems to result in another distinctive feature of YBCO, namely, a plateau or a bump (see table) on the $\lambda_{ab}(T)$ curve, which has been observed in high-quality YBCO single crystals [8–12] and films [16, 41]. However, recent measurements of $\Delta\lambda_{ab}(T)$ in the YBCO crystals [14] grown in a high-purity $BaZrO_3$ crucible do not show such features in the intermediate temperature range. The authors of [14] argue that the disagreement with the results of [9] arises from a problem related with the surface of the crystal. The last observation still lacks a convincing explanation.

Finally, another feature in the *T*-dependence of the impedance of high-quality YBCO crystals was detected: a noticeable increase of $R_s(T)$ with an increasing temperature (a shoulder) at temperatures larger than the peak (30 K). It turns out that this shoulder is reproducible in the experiments [9, 11]. Similarly, an explanation of this observation is lacking.

Surface impedance $Z_s(T) = R_s(T) + iX_s(T)$ in the *ab*-plane of high-T_c single crystals at frequencies ~10 GHz

HTSC	Superconducting state, $T < T_c$			Normal state $1.5T_c > T \geq T_c$
	low temperatures $4\ \text{K} < T \ll T_c$	intermediate temperatures $T \sim T_c/2$	$T \longrightarrow T_c$	
Orthorhombic structure YBCO $T_c \approx 92$ K	$\Delta R_s(T) \propto T, \Delta X_s(T) \propto T$ at $T \leq T_c/4$; Essentially different slopes of $\Delta\lambda(T) \propto T$ [1–14]	Broad peak in $R_s(T)$ at $25 < T < 45$ K [4–14, 57–60] Peculiarities: 1. Shoulder [9, 11] in $R_s(T)$ at $T > 40$ K; 2. Bump [9] or plateau [8, 10] on the curves of $X_s(T)$ at $50 < T < 80$ K	Different slope of $\lambda(T)$ [3–14]	Normal skin-effect
Tetragonal structure BSCCO $T_c \approx 90$ K [19–22] TBCO $T_c \approx 80$ K [23, 24] TBCCO $T_c \approx 110$ K [10, 12]	$\Delta R_s(T) \propto T, T \leq T_c/2$ $\Delta X_s(T) = \omega\mu_0\Delta\lambda(T) \propto T, T \leq T_c/3$		Rapid growth of $R_s(T)$ and $X_s(T)$	$R_s(T) = X_s(T) = \sqrt{\omega\mu_0\rho(T)/2}$ $\Delta\rho(T) \propto T$

2.2. Complex Conductivity

Equations (2)–(4) allows us to express the real and imaginary parts of the complex conductivity $\sigma_s = \sigma_1 - i\sigma_2$ in terms of R_s and X_s as

$$\sigma_1 = \frac{2\omega\mu_0 R_s X_s}{(R_s^2 + X_s^2)^2}, \quad \sigma_2 = \frac{\omega\mu_0(X_s^2 - R_s^2)}{(R_s^2 + X_s^2)^2}. \qquad (6)$$

Above the superconducting transition temperature, the mean free path l of current carriers is shorter than the skin depth δ_n in the normal state (for $T \geq T_c$, $l \ll \delta_n$), which corresponds to the conditions of the normal skin effect. Equations (2)–(4) and (6) also apply to the normal state of HTSC's, where $R_n(T) = X_n(T) = \sqrt{\omega\mu_0/2\sigma_n(T)}$ with $\sigma_n \equiv \sigma_1$ ($T > T_c$) and $\sigma_2 \ll \sigma_1$ at microwave frequencies.

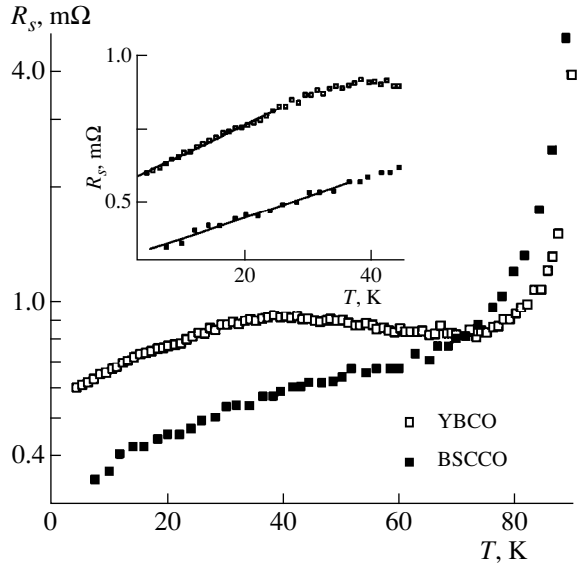

Fig. 2. Comparison of the temperature dependence of the surface resistance $R_s(T)$ of BSCCO and YBCO single crystals at 14.4 GHz. Experimental data are taken from [21] (BSCCO at 14.4 GHz) and [8] (YBCO at 9.4 GHz, scaled by ω^2 to 14.4 GHz). The inset shows the linear T-dependence of R_s at low T for both materials and a broad peak of $R_s(T)$ for YBCO.

The components $\sigma_1(T)$ and $\sigma_2(T)$ are not measured directly but can be derived from measurements of $R_s(T)$ and $X_s(T)$ using Eq. (6).

2.2.1. Low-temperature region ($T \ll T_c$). When $R_s(T) \ll X_s(T)$, Eq. (6) reduces to

$$\sigma_1(T) = \frac{2\omega\mu_0 R_s(T)}{X_s^3(T)}, \quad \sigma_2(T) = \frac{\omega\mu_0}{X_s^2(T)}. \qquad (7)$$

It then follows from Eq. (7) that for low and intermediate temperatures, $\sigma_1/\sigma_2 = 2R_s/X_s \ll 1$. The increments $\Delta\sigma_1(T)$ and $\Delta\sigma_2(T)$ depend on the increments $\Delta R_s(T)$ and $\Delta X_s(T)$ relative to the respective quantity:

$$\Delta\sigma_1 \propto \left(\frac{\Delta R_s}{R_s} - 3\frac{\Delta X_s}{X_s}\right), \quad \Delta\sigma_2 \propto -\frac{\Delta X_s}{X_s}. \qquad (8)$$

It follows from Eq. (8) that the dominant changes of $\sigma_2(T)$ are determined mainly by the function $X_s(T) = \omega\mu_0\lambda(T)$, which reflects the T-dependence of the magnetic field penetration depth.

The T-dependence of the real part of the conductivity, $\sigma_1(T)$, is determined by the competition between the increments $\Delta R_s/R_s$ and $\Delta X_s/X_s$.

In conventional superconductors, the quantity $X_s(T)$ ($\gg R_s$) is practically T-independent ($\Delta X_s \approx 0$) at temperatures $T \leq T_c/2$, and $R_s(T)$ decreases exponentially and approaches the residual surface resistance R_{res} as $T \longrightarrow 0$. By subtracting R_{res} from the measured $R_s(T)$, we obtain, using Eqs. (7) and (8), the temperature dependence of

$\sigma_1(T)$ predicted by the BCS theory: $\sigma_1 = 0$ at $T = 0$ and, for $T \le T_c/2$, $\Delta\sigma_1(T)$ shows an exponentially slow growth with an increasing temperature. We note that the smallest value of R_{res} detected in pure Nb is at least two orders of magnitude smaller than the smallest value of R_{res} measured in YBCO. The extremely small values of the surface resistance in Eq. (8) indicate that the increment $\Delta\sigma_1(T)$ is always positive in classical superconductors ($\Delta\sigma_1(T) > 0$), at least in the temperature interval $T < 0.8\ T_c$, before the maximum of the BCS coherence peak is reached.

For HTSC single crystals, the T-dependence of $\Delta\sigma_1(T)$ is radically different from that predicted by the theories of the microwave response of conventional superconductors. For $T < T_c$, the increments $\Delta R_s(T)$ and $\Delta X_s(T)$ in HTSC's are not small; in addition, $\Delta X_s(T) \gg \Delta R_s(T)$. Although $R_s(T) < X_s(T)$, $\Delta R_s/R_s$ is not necessarily greater than $3\Delta X_s/X_s$ in Eq. (8) or positive at all temperatures. When that occurs, $\sigma_1(T)$ increases with a decreasing temperature. The function $\sigma_1(T)$ is maximum at some $T = T_{max}$, and then $\sigma_1(T)$ becomes smaller with a decreasing temperature. $\sigma_1(T)$ has a peak if the value of R_{res} is sufficiently small as $T \longrightarrow 0$:

$$R_{res} < \frac{X_s(0)}{3}\frac{\Delta R_s(T)}{\Delta X_s(T)}. \qquad (9)$$

If inequality (9) is satisfied, T_{max} is a finite temperature, while for R_{res} being equal to the right-hand side of (9), T_{max} shifts to 0 K. If R_{res} is such that (9) is not satisfied, $\sigma_1(T)$ decreases at low temperatures as the temperature is increased, which is quite different from that observed in conventional superconductors.

Thus, the shape of $\sigma_1(T)$ for $T \ll T_c$ depends on the value of the residual surface resistance R_{res}, whose origin and accurate value are unknown. For this reason, the shapes of the $\sigma_1(T)$ curves are not determined unambiguously for $T \le T_c/2$, unlike the functions $R_s(T)$ and $X_s(T)$, which are directly measured in experiments.

If we linearly extrapolate $R_s(T)$ to $T = 0$ and attribute the resulting value $R_s(0)$ to the residual surface resistance ($R_s(0) = R_{res}$) and then substitute the temperature-dependent difference $R_s(T)$–R_{res} into the numerator of the first expression in Eq. (7), the result is that the $\sigma_1(T)$ curve has a broad peak for HTSC materials. Near $T = 0$, $\sigma_1(T)$ increases linearly with T from zero, reaches a maximum at T_{max}, and then decreases to $\sigma(T_c)$. This procedure, however, ignores the possibility of intrinsic residual losses. Therefore, some authors (see, e.g., [14, 21, 59]) associate residual losses in HTSC single crystals with a residual normal electron fluid. This implies that the source of the residual loss is in the bulk of the sample, although it is probably not intrinsic. If this contribution is excluded from the complex conductivity of the superconductor, one obtains $\sigma_1(T = 0) \longrightarrow 0$, as can be seen in Fig. 3 from the measurements taken at 13.4, 22.7, and 75.3 GHz in [14]. The peak of $\sigma_1(T)$ shifts to higher temperatures, and its size diminishes as the experimental frequency is increased. In YBCO single crystals, the temperature T_{max} at which the maximum of σ_1 occurs is close to the temperature at which the peak of $R_s(T)$ occurs.

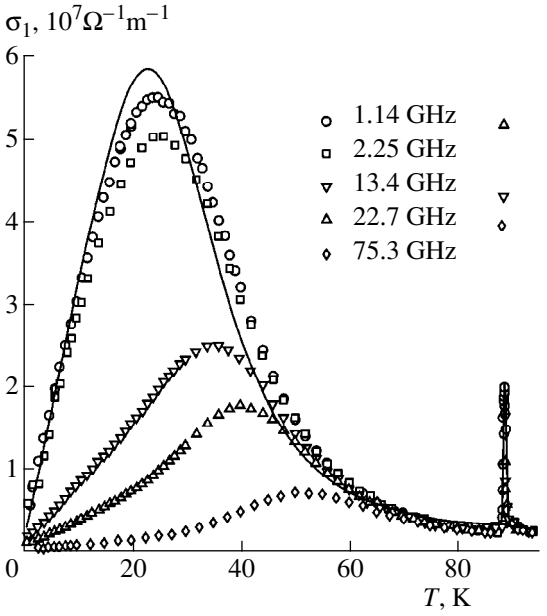

Fig. 3. Real part of the conductivity $\sigma_1(T)$ of YBCO single crystal at different frequencies [14]. The data (symbols) are the courtesy of the Vancouver group (D.A. Bonn). Solid line is the T-dependence of $\sigma_1(T)$ at 1.14 GHz calculated using the modified two-fluid model and taking the inhomogeneous broadening of the superconducting transition into account ($\delta T_c = 0.4$ K in Eq. (21), see Section 3.3).

Finally, one can procure $\sigma_1(T)$ from measurements of $R_s(T)$ and $X_s(T)$ for $T > 0$ without any concern about R_{res}. In this case, $\sigma_1(0)$ is not determined uniquely. Whether $\sigma_1(T)$ has a peak depends on the validity of condition (9). The curves at 1 and 2 GHz in Fig. 3 were obtained using Eq. (6) without subtracting any residual losses.

2.2.2. Temperatures close to T_c ($T \longrightarrow T_c$). Equations (7) and (8) do not apply near T_c. In this temperature range, it is necessary to use the general local relations (2)–(4) and (6).

The conductivity $\sigma_2(T)$ in the *ab*-plane of HTSC crystals abruptly drops to very small values in the normal state. The expression $[T_c/\sigma_2(0)]d\sigma_2(T)/dT$ at $T = T_c$ that defines the slope of $\lambda^2(0)/\lambda^2(T)$ at $T = T_c$ varies between –2 and –4 for different crystals.

The real part of the conductivity, $\sigma_1(T)$, does not show a coherence peak near $T = 0.85T_c$, as predicted by BCS. Usually, the real part of the conductivity of HTSC single crystals has a narrow peak near T_c, which increases with decreasing the frequency [21, 23, 24].

The width of the narrow peak of $\sigma_1(T)$ coincides with the width of the $R_s(T)$ transition at microwave frequencies. A possible explanation of the sharp peak just below T_c is an inhomogeneous broadening of the superconducting transition [77–79] or the fluctuation effects [24, 80, 81].

3. MODIFIED TWO-FLUID MODEL

As was shown in [65], high T_c values ($T_c \sim 100$ K), the temperature dependence of the resistivity, the frequency dependence of the momentum relaxation time, and other properties of the normal state in optimally doped HTSC's are well described within the framework of the Fermi-liquid approach involving strong electron–phonon coupling (SC) [63]. The SC model also explains some of the features of the superconducting state of HTSC's. It follows from the Eliashberg theory that the distinctive property of superconductors with strong coupling is that the gap in the spectrum of electronic excitations is smeared. Strictly speaking, there is no gap whatsoever at $T \neq 0$ [82, 83]. This leads to breaking of Cooper pairs, smearing of the peak in the density of states at $\hbar\omega = \Delta(T)$ due to the inelastic scattering of electrons by thermally excited phonons, and suppression of coherence effects. As a result, the amplitude of the coherence peak decreases and, according to [84, 85], virtually disappears at frequencies around 10 GHz if the electron–phonon coupling constant exceeds unity. Moreover, the quasiparticle generation mechanism is radically different from that of the BCS model. The quasiparticles are generated without jumps across the energy gap and can be in states with all energies down to $\hbar\omega = 0$. These states can be classified as gapless, and the quasiparticles can be treated [65] as normal current carriers in the two-fluid model. Thus, it is not surprising that an important consequence of the SC model is the nonexponential behavior of $R_s(T)$ [86] and $\lambda(T)$ [87]. Power-law temperature dependences were also predicted by the two-fluid Gorter–Casimir (GC) model [76]; near T_c, they proved to be quite close to the results of calculations performed in the SC model. In particular, the curves $\lambda^2(0)/\lambda^2(T)$ calculated by the SC model [88–91] proved to be sufficiently close to the function $n_s(t)/n = 1 - n_n(t)/n = 1 - t^4$ in the GC model. At $T = T_c$, the slopes of these curves are in agreement with those measured with different YBCO single crystals and are equal to –3 [4] or –4 [5, 8, 10]. The experimental fact that there is no BCS coherence peak in the conductivity of HTSC crystals indicates the necessity of taking the strong coupling effects near T_c into account and the feasibility of interpreting HTSC properties at microwave frequencies in terms of a two-fluid model.

Complex conductivity σ_s is a basic property of superconductors. In accordance with the GC model [76], the expressions for the components of $\sigma_s = \sigma_1 - i\sigma_2$ are

$$\sigma_1 = \frac{n_n e^2 \tau}{m}\left[\frac{1}{1+(\omega\tau)^2}\right],$$
$$\sigma_2 = \frac{n_s e^2}{m\omega}\left[1 + \frac{n_n}{n_s}\frac{(\omega\tau)^2}{1+(\omega\tau)^2}\right]. \quad (10)$$

At temperatures $T \leq T_c$, the total carrier concentration is $n = n_s + n_n$, where $n_{s,n}$ are the fractions of the superconducting and normal carrier densities (both have the same charge e and effective mass m). The real part σ_1 is determined solely by the normal component, while both components (normal and superconducting) contribute to the imaginary part σ_2. In the GC model, the relaxation time τ of normal carriers is independent of the temperature. This is acceptable if we assume that the behavior of normal carriers in superconductors is similar to that of normal carriers in normal metals at low temperatures. Scattering of electrons at very low temperatures is due to impurities and is independent of the temperature. Therefore, the temperature dependence of the real part of the conductivity (10) in the GC model is determined entirely by the function $n_n(T)$ with $n_s(T) = n - n_n(T)$ only.

For sufficiently low frequencies $(\omega\tau)^2 \ll 1$, the expressions of the conductivity components in Eq. (10) transform into simple relations

$$\sigma_1 = \frac{e^2\tau}{m}n_n, \quad \sigma_2 = \frac{e^2}{m\omega}n_s = \frac{1}{\mu_0\omega\lambda^2}, \quad (11)$$

where $\lambda = \sqrt{m/\mu_0 n_s e^2}$ is the London penetration depth of a static magnetic field.

Penetration of alternating fields into superconductors is controlled by the frequency-dependent skin depth. Using complex conductivity (11), one obtains the complex skin depth δ_s by generalizing the corresponding expression for a normal conductor:

$$\delta_s = \frac{\sqrt{2}\lambda}{\sqrt{\omega\tau(n_n/n_s) - i}}. \quad (12)$$

With an increasing angular frequency ω, the skin depth $\mathrm{Re}\,\delta_s$ decreases; therefore, the London penetration depth λ gives the upper bound for the penetration of the electromagnetic field into a superconductor. In the GC model, the λ value diverges near T_c as $\lambda(t) = \lambda/(2\sqrt{1-t})$ and the function $\sigma_2(t)/\sigma_2(0) = 4(1-t)$ tends linearly to zero at $T = T_c$ with a slope equal to –4. At the same time, at $T = T_c$, the skin depth $\mathrm{Re}\,\delta_s$, defined by Eq. (12), crosses over to the skin depth δ_n for a normal conductor.

3.1. Scattering and Surface Resistance of HTSC Single Crystals

In conventional superconductivity, one assumes that the mean free path does not vary with the temperature below T_c. In a normal metal at much higher temperatures than the corresponding T_c of a conventional superconductor, the electron scattering rate is proportional to T [92]. Since the transition temperatures of HTSC's are much larger than those of conventional superconductors, it stands to reason that temperature affects the electron scattering rate of the quasiparticles of HTSC's below T_c but is limited to a constant rate at low temperatures. Therefore, if a two-fluid model is to be successful in explaining transport properties of HTSC's, it is natural to include a temperature variation of τ into that model.

To obtain an expression for $\tau(T)$, we rely on the analogy between the "normal fluid" component in the superconducting state and charge carriers in a normal metal. According to Mathissen's rule, the reciprocal relaxation time at temperatures below the Debye temperature Θ is

$$\frac{1}{\tau} = \frac{1}{\tau_{imp}} + \frac{1}{\tau_{e-ph}}. \tag{13}$$

The first term on the right-hand side is due to impurity scattering and is independent of temperature, and the second is due to the electron–phonon scattering and is proportional to T^5.

From Eq. (13), we express $\tau(T)$ as

$$\frac{1}{\tau(t)} = \frac{1}{\tau(T_c)}\frac{\beta + t^5}{\beta + 1}, \tag{14}$$

where β is a numerical parameter ($\beta \approx \tau(T_c)/\tau(0)$), provided this ratio is much less than unity. It must be pointed out, however, that this approximation is not always satisfied.

Equation (14) corresponds to the low-temperature limit of the Bloch–Grüneisen formula, which includes impurity scattering and can be presented over a wide temperature range by the expression

$$\frac{1}{\tau(t)} = \frac{1}{\tau(T_c)}\frac{\beta + t^5 \mathcal{J}_5(\kappa/t)\mathcal{J}_5(\kappa)}{\beta + 1},$$
$$\mathcal{J}_5(\kappa/t) = \int_0^{\kappa/t} \frac{z^5 e^z dz}{(e^z - 1)^2}, \tag{15}$$

where $\kappa = \Theta/T_c$. For $T < \Theta/10$ ($\kappa > 10t$), Eq. (15) approaches the form of Eq. (14). For $T > \Theta/5$ ($\kappa < 5t$), we obtain from Eq. (15) the linear T-dependence $1/\tau(t) \propto t$. Examples of $1/\tau(t)$ for different parameters of β, κ, and $\tau(T_c)$ are shown in Fig. 4.

For $\omega\tau(T_c) \ll 1$, which is normally satisfied at microwave frequencies in HTSC's, the parameter

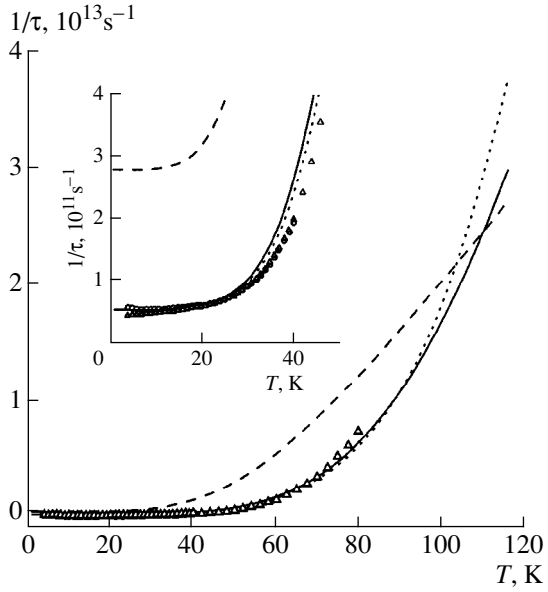

Fig. 4. Scattering rate of quasiparticles calculated form Eq. (14), dotted line: $\beta = 0.005$, and Eq. (15), solid line: $\beta = 0.005$, $\kappa = 9$; dashed line: $\beta = 0.02$, $\kappa = 4$. The triangles are calculated from $1/\tau = [1 - \lambda^2(0)/\lambda^2(T)]/[\mu_0\sigma_1(T)\lambda^2(0)]$, with $\sigma_1(T)$ and $\lambda(T)$ at 1.14 GHz and $\lambda(0) = 1600$ Å in the *ab*-plane, with the currents parallel to the *a*-direction of the YBCO crystal [14]. The inset shows the low-temperature parts of the curves. The circles are from Fig. 8 of [14].

$\omega\tau(T_c)$ is obtained from measurements of $R_s(T_c)$ and $X_s(0)$:

$$\omega\tau(T_c) = \frac{X_s^2(0)}{2R_s^2(T_c)} = \frac{\sigma_1(T_c)}{\sigma_2(0)}. \tag{16}$$

At frequencies ≈10 GHz, the value of $\omega\tau$ for the best HTSC crystals is of the order of 10^{-3} at $T = T_c$ and remains less than unity at all temperatures $T < T_c$, as is discussed in what follows. In the two-fluid model, therefore, the expressions of the conductivity components in Eq. (10) turn into the simple form (11).

All experimental data of $R_s(T)$ for high-quality HTSC single crystals can be elucidated by our two-fluid model with $\tau(T)$ given by Eqs. (14) or (15).

Measurements of $R_s(T)$ of YBCO single crystals at frequencies of order or less than 10 GHz are analyzed first. The values of $\sigma_2(T)/\sigma_2(0) = \lambda^2(0)/\lambda^2(T) = n_s(T)/n$ measured in the same experiments and those of $\sigma_1(T)/\sigma(T_c)$ obtained from Eq. (11) are substituted into Eq. (3). We then use the relation $n_n(T)/n = 1 - \sigma_2(T)/\sigma_2(0)$, which is obtained from the experimental data, and take $\tau(T)$ from Eqs. (14) or (15).

Setting $\beta = 0.005$ and $\kappa = 9$ in Eq. (15) and taking the experimental values $\sigma_2(T)/\sigma_2(0)$ from Fig. 11 (see below) and $\omega\tau(T_c) = 7.5 \times 10^{-4}$ at 1.14 GHz, we find from Eqs. (11) and (3) the T-dependence of $R_s(T)$, shown by the curves in Fig. 5. These curves match the

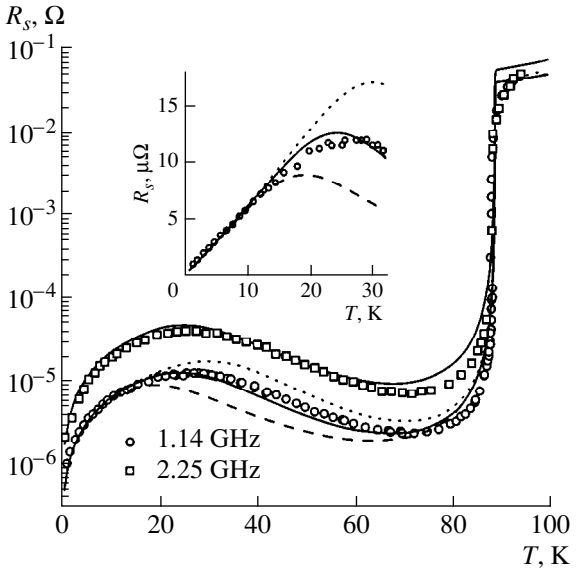

Fig. 5. Experimental $R_s(T)$ data of YBCO single crystal [14] at 1.14 GHz (circles) and 2.25 GHz (squares). Solid curves are calculations using Eqs. (3), (11), and (14). The dashed curves are calculated at 1.14 GHz with the term t^5 replaced by t^4 in the numerator of Eq. (14); the dotted curves, with t^6. The inset shows a linear plot of $R_s(T)$ at low temperatures at 1.14 GHz.

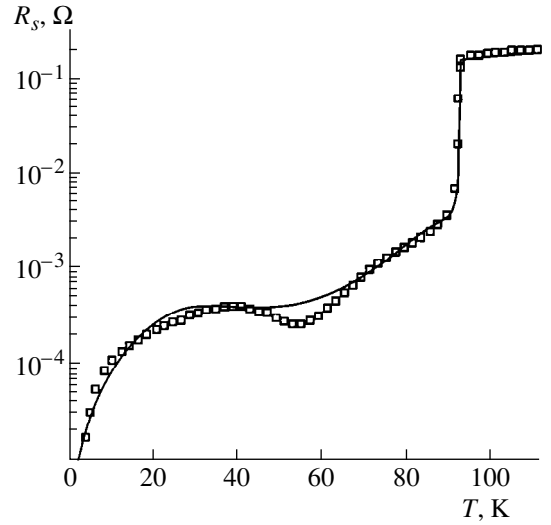

Fig. 6. Comparison between the calculated (solid line) and measured (squares) surface resistance $R_s(T)$ of YBCO single crystal at 10 GHz. Experimental data are from [9].

data of [14] over the entire temperature range. The same result is obtained using Eq. (14) instead of Eq. (15), with $\beta = 0.005$. For $\kappa \gg 1$ and $T \lesssim T_c$, Eqs. (14) and (15) are identical.

It follows from Eqs. (5) and (11) that for $\alpha t \ll 1$ [see Eq. (1)], a rough estimate of the temperature t_m at which $R_s(T)$ is maximum is obtained from the relation $\beta \simeq 4t_m^5$. The value of $\tau(0)$ is found from the slopes dR_s/dT and dX_s/dT of the experimental data of $R_s(T)$ and $X_s(T)$ as $T \longrightarrow 0$ ($\omega\tau(0) < 1$):

$$\omega\tau(0) = \left.\frac{dR_s}{dX_s}\right|_{T \to 0}. \qquad (17)$$

With Eqs. (16) and (17), the parameter $\beta \approx \tau(T_c)/\tau(0)$ is determined from the surface impedance data. As β increases, the maximum and minimum of $R_s(T)$ change into an inflection point with horizontal tangent; for larger β, the maximum of $R_s(T)$ disappears completely [74].

The linear growth of $R_s(T)$ with T at low temperatures (inset in Fig. 5) is a direct consequence of the linear change of $\lambda(T)$ near $T = 0$, which is proportional to the coefficient α in Eq. (1), and is the result of a constant scattering rate at low temperatures, as shown in Fig. 4.

The dashed and dotted curves shown in Fig. 5 are the calculated $R_s(T)$ values at 1.14 GHz, with t^5 replaced by t^4 (dashed curve) and by t^6 (dotted curve) in Eq. (14). The best fit of the experimental data is $1/\tau(t) \propto t^5$. Moreover, Eq. (15) enables us to incorporate the shoulder of $R_s(T)$ obtained with YBCO single crystals in [9, 11]. This is shown in Fig. 6, which contains measurements (squares) of $R_s(T)$ at 10 GHz taken from [9] and calculations (solid line) of $R_s(T)$ based on Eqs. (11) and (3) with $\omega\tau(T_c) = 4 \times 10^{-3}$, $\sigma_2(T)/\sigma_2(0)$ obtained from the same experimental data [9], $\beta = 0.02$, and $\kappa = 4$ in Eq. (15).

The calculated curves in Figs. 5 and 6 are very close to the experimental data and display the following common and unique features of $R_s(T)$ for $T < T_c$ and $\omega\tau < 1$ of high-quality YBCO single crystals fabricated by different methods: (i) the linear temperature dependence of the surface resistance, $\Delta R_s(T) \propto T$, caused by the linear variation of $\Delta X_s(T) \propto \Delta\lambda_{ab}(T) \propto T$ at temperatures $T \ll T_c$ and by the limit $\tau(T) \longrightarrow$ const at low temperatures; (ii) the broad peak of $R_s(T)$ in the intermediate temperature range due to the rapid decrease of the relaxation time $\tau(T) \propto T^{-5}$ with an increasing temperature; and (iii) the increase in $R_s(T)$ in the range $T_c/2 < T < T_c$ (Fig. 6) caused by the crossover from T^{-5} to T^{-1} of $\tau(T)$ in Eq. (15), which occurs in Fig. 6 at a lower temperature than in Fig. 5. The behavior of $1/\tau(T)$ for these two YBCO crystals is shown in Fig. 4.

Up to this point, we did not take the residual surface resistance R_{res} of the samples into account. In the YBCO crystals, whose data are plotted in Figs. 5 and 6 scaled to the same frequency (10 GHz), the resistance is $R_{res} < 50$ μΩ. $R_{res}/R(T_c) < 10^{-3}$ is so small that R_{res} was neglected even at $T \ll T_c$. In most HTSC crystals that were investigated, however, $R_{res}/R(T_c) > 10^{-3}$ (see, e.g., Figs. 1 and 2). Therefore, it is important that R_{res} is

added to the calculated $R_s(T)$ values when comparing the latter with the experimental data.

Figure 7 compares the measured $R_s(T)$ and $X_s(T)$ of BSCCO, plotted in Fig. 1, with the results of calculations based on Eqs. (3) and (4). In this case, we added the constant $R_{res} = 0.5$ mΩ to the calculated values of $R_s(T)$. The calculations are based on measurements of $\sigma_2(T)/\sigma_2(0)$ obtained in the same experiment and are plotted in the inset to Fig. 13 (see below), with the parameters $\omega\tau(T_c) = 0.9 \times 10^{-2}$, $\beta = 2$ and $\kappa = 3$ in Eq. (15). It is clear that the agreement between the calculated and experimental curves is good throughout the temperature interval $5 \le T \le 120$ K.

Another reason for including R_{res} is the ratio $R_{res}/R(T_c) \propto \omega^{3/2}$. Figure 8 is based on the experimental data of BSCCO single crystal measured in [21] at three frequencies: 14.4 ($\omega\tau(T_c) = 0.7 \times 10^{-2}$), 24.6, and 34.7 GHz. The solid curves are the calculations at these frequencies obtained from Eqs. (11) and (3) using $\tau(T)$ from Eq. (15) with $\beta = 0.1$ and $\kappa = 4$. The comparison procedure is different from that discussed above for YBCO crystals because $R_{res} \propto \omega^2$ is added to the calculated $R_s(T)$ values. The inset of Fig. 8 shows a linear plot of the measured and calculated surface resistance at low temperatures. We emphasize that at temperatures below $T_c/2$, the value of $\Delta R_s(T)$ is proportional to T.

In the millimeter and shorter wavelength bands, the condition $\omega\tau < 1$ may not be satisfied in the superconducting state of the purest HTSC single crystals because of the fast growth of $\tau(T)$ with decreasing $T < T_c$. In analyzing the experimental data of $Z_s(T)$ and $\sigma_s(T)$, therefore, it is natural to not only take R_{res} into account but also to use the more general Eq. (10) of the two-fluid model to replace Eq. (11). The $R_s(T)$ data of [14] at the frequencies of 13.4, 22.7, and 75.3 GHz are shown in Fig. 9 with the calculated $R_s(T)$ values (obtained on the same YBCO crystal that was used in Fig. 5). We used $\tau(T_c)/\tau(0) \approx \beta = 5 \times 10^{-3}$ in Eq. (14) for all curves shown in Fig. 9 (the same as previously used in Fig. 5) and added $R_{res} = 0.3$ mΩ to $R_s(T)$ [Eq. (3)] at 75.3 GHz only. The conductivity components $\sigma_1(T)$ and $\sigma_2(T)$ involved in Eq. (3) are obtained from the experimental data of $\sigma_2(T)/\sigma_2(0)$ at 1.14 GHz [14] (shown in Fig. 11) and from Eq. (10).

Figure 10 shows another example. The experimental $R_s(T)$ data (squares) of a TBCO single crystal ($T_c = 78.5$ K) [23] are compared with the results of calculations based on Eqs. (3), (10), and (15). The curve representing the theoretical values $R_s(T) + R_{res}$ is plotted using $\beta = 0.1$, $\kappa = 5.5$, $\omega\tau(T_c) = 1.7 \times 10^{-2}$, $R_{res} = 0.8$ mΩ, and with $\sigma_2(T)/\sigma_2(0)$ shown in the inset (circles) of Fig. 10.

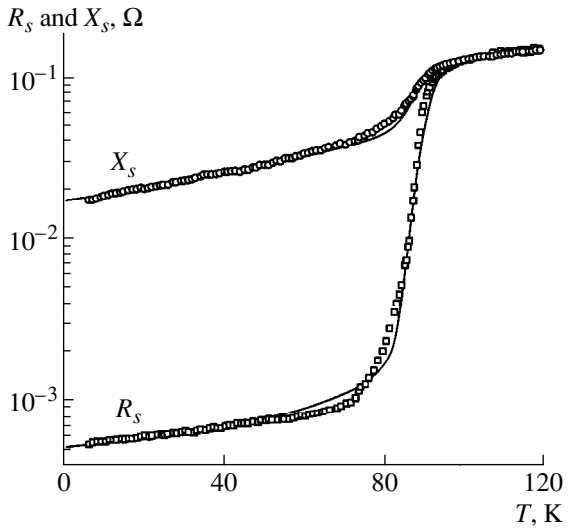

Fig. 7. Comparison between the calculated (solid lines) and measured surface impedance (symbols) of BSCCO single crystal (see Fig. 1). A constant $R_{res} = 0.5$ mΩ is added to the values of $R_s(T)$obtained from Eq. (3).

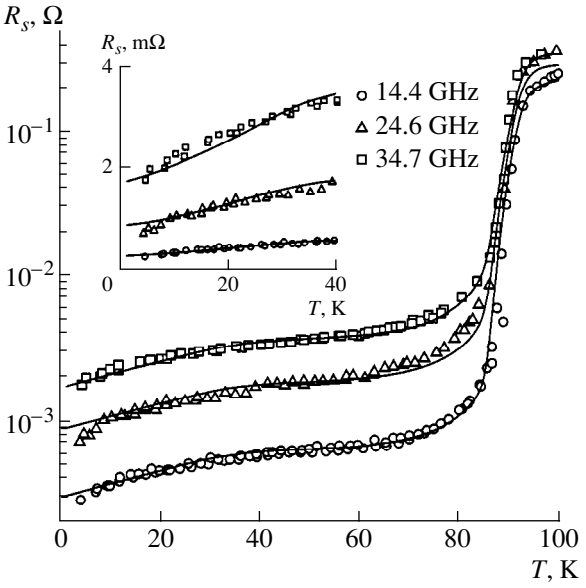

Fig. 8. Experimental data of the BSCCO single crystal [21] at various frequencies: 14.4 GHz (circles), 24.6 GHz (triangles), and 34.7 GHz (squares). The solid curves are the calculated $[R_s(T) + R_{res}]$-functions, with the respective R_{res} value of 0.29, 0.85 and 1.7 mΩ. The inset shows the linear temperature dependences of the surface resistance at low temperatures.

3.2. Temperature Dependence of the Superconducting Electron Density

In the previous section, we accentuated that the modified two-fluid model describes all features of the surface resistance $R_s(T)$ of different HTSC's over a wide frequency range with only one parameter (k). This

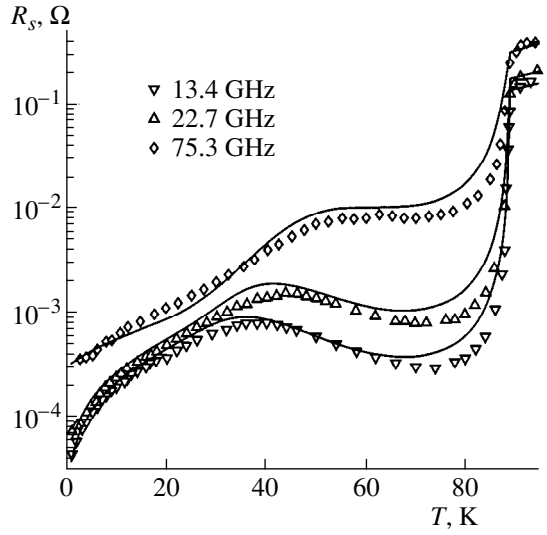

Fig. 9. Comparison between the calculated (lines) and measured [14] (symbols) surface resistance $R_s(T)$ of the YBCO single crystal at 13.4, 22.7, and 75.3 GHz. We assumed $R_{res} = 0.3$ mΩ for 75.3 GHz, zero for the other frequencies.

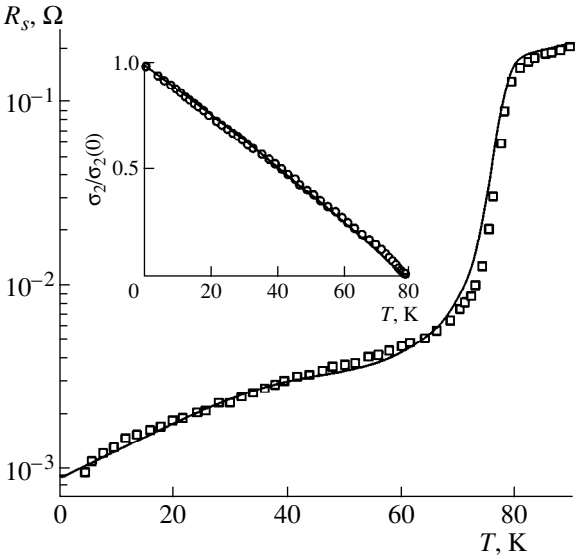

Fig. 10. Surface resistance $R_s(T)$ of a TBCO single crystal at 24.8 GHz taken from [23]. Solid curve is the calculated $[R_s(T) + R_{res}]$-function with $R_{res} = 0.8$ mΩ. The inset shows the measured [23] (circles) and calculated results of $\sigma_2(T)/\sigma_2(0)$ (solid line) using Eq. (18) with $\alpha = 0.9$.

was done using the measured (known from the same experiment) T-dependences of the superconducting electron density $\lambda_{ab}^{-2}(T)$. However, we think that our phenomenological model would be incomplete unless simple formulas are available that correctly describe the measurements of $\Delta\lambda_{ab}(T)$. Figures 10 (the inset), 11, and 12 show $\sigma_2(T)/\sigma_2(0) = \lambda^2(0)/\lambda^2(T) = n_s(T)/n$ in the *ab*-plane of TBCO, YBCO, and BSCCO single crystals from [23, 14, 21], respectively. All of these quantities change linearly with temperature at low temperatures and can be approximated by the function [73]

$$n_s/n = (1-t)^{\alpha}, \qquad (18)$$

where α is a numerical parameter. For $t \ll 1$, Eq. (1) follows from Eq. (18). For the cited experiments, the values of α fall into the range $0.4 < \alpha \le 0.9$. Near T_c, we obtain $\lambda(t) \propto n_s(t)^{-1/2} \propto (1-t)^{-\alpha/2}$, which is also in reasonably good agreement with the experimental data. However, Eq. (18) yields an infinite value of the derivative $d\sigma_2(t)/dt \propto (1-t)^{\alpha-1}$ at $t = 1$ for $\alpha < 1$.

An approximation for $n_s(t)/n$ proposed in [75] is close to Eq. (18),

$$n_s/n = 1 - \alpha t - (1-\alpha)t^6, \qquad (19)$$

and is shown by solid lines in Figs. 11 and 12. Equation (19) insures that the slope of $\lambda^2(0)/\lambda^2(t)\big|_{T_c} = 5\alpha - 6$ at T_c is finite and negative for $\alpha < 1.2$.

However, the above functions for $n_s(t)$ in their simplest forms (18) and (19) do not account for all features in $\lambda^2(0)/\lambda^2(T)$ detected recently in YBCO crystals (see table) in the intermediate temperature range [8–11]. Moreover, the slope of these curves at $T \ll T_c$ requires that $\alpha > 1$ in Eq. (18), which would lead to a zero slope of the $\sigma_2(T)/\sigma_2(0)$ curve $T = T_c$. Therefore, we have added an additional empirical term to the right-hand

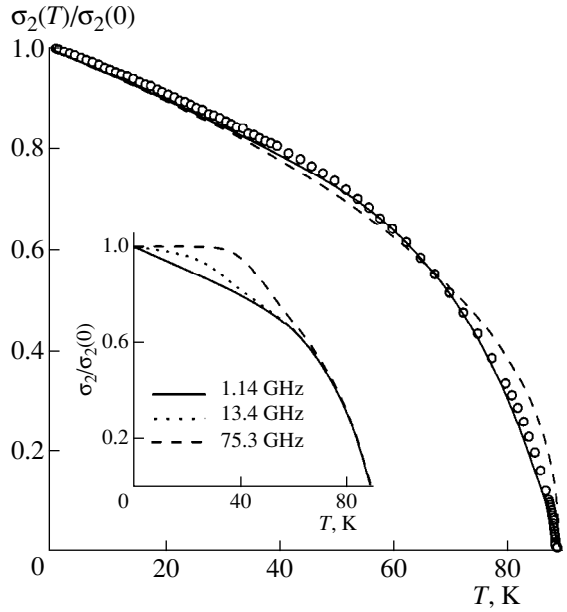

Fig. 11. Plots of Eq. (18) (dashed line, $\alpha = 0.42$) and Eq. (19) (solid line, $\alpha = 0.47$), showing the fit to the empirical $\sigma_2(T)/\sigma_2(0)$. The experimental data (circles) are from [14] at 1.14 GHz. The inset shows the temperature dependences of $\sigma_2(T)/\sigma_2(0)$ at various frequencies calculated from Eqs. (10), (19) and (14).

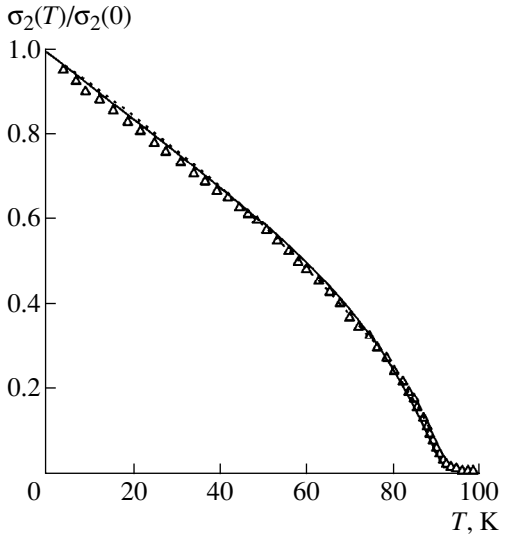

Fig. 12. Comparison between the calculated (solid curve: Eq. (19), $\alpha = 0.74$; dotted line: Eq. (18), $\alpha = 0.7$) and measured [21] (symbols) of the $\sigma_2(T)/\sigma_2(0)$ values of BSCCO single crystal [75].

side of Eq. (18) without violating the particle conservation condition $n_s + n_n = n$:

$$n_s/n = (1-t)^{\alpha}(1-\delta) + \delta(1-t^{4/\delta}), \qquad (20)$$

where $0 < \delta < 1$ is the weight factor. For $\delta \ll 1$ and $\alpha > 1$, the dominant contribution to $\sigma_2(T)$ throughout the relevant temperature range is still due to the first term on the right-hand side of Eq. (20), while the second is responsible for the finite slope of $\sigma_2(T)/\sigma_2(0)$ at $T = T_c$, which is equal to –4 in accordance with the GC model. As δ increases, the second term on the right-hand side of Eq. (20) becomes more essential. The experimental curve of $\sigma_2(T)/\sigma_2(0)$ derived from the $R_s(T)$ and $X_s(T)$ measurements of the YBCO crystal in [8] is properly described by Eq. (20) with $\delta = 0.5$ and $\alpha = 5.5$ (Fig. 13). This calculation reflects the characteristic features of the experimental data, namely, the linear section of n_s and the positive second derivative ($\alpha > 1$) in the low-temperature region, the plateau in the intermediate temperature range, and the correct value of the slope near T_c.

Using Eq. (20) with $\alpha = 2$ and $\delta = 0.2$, we can also describe the T-dependence of $\sigma_2(T)$ of BSCCO crystals (Figs. 1 and 7), plotted in the inset to Fig. 13.

3.3. The Real Part of the Conductivity

Since the measurements and calculations of $R_s(T)$, $X_s(T)$, and $\sigma_2(T)$ are in good agreement and consistent with $\sigma_1(T)$ in the range $T < T_c$, the modified two-fluid model can be a powerful tool in describing the electrodynamic properties of HTSC's. The only feature that has not been investigated by this model is the behavior of $Z_s(T)$ and $\sigma_s(T)$ in the temperature range near T_c. A spectacular display is the narrow peak in the real part of the conductivity (see Fig. 3).

The narrow peak near T_c can be described by an effective medium model [79, 93] that takes the inhomogeneous broadening of the superconducting transition into account. We assume that different regions of a given specimen experience transitions to the superconducting state at different temperatures within the T-range δT_c. If the dimension of each of these regions is smaller than

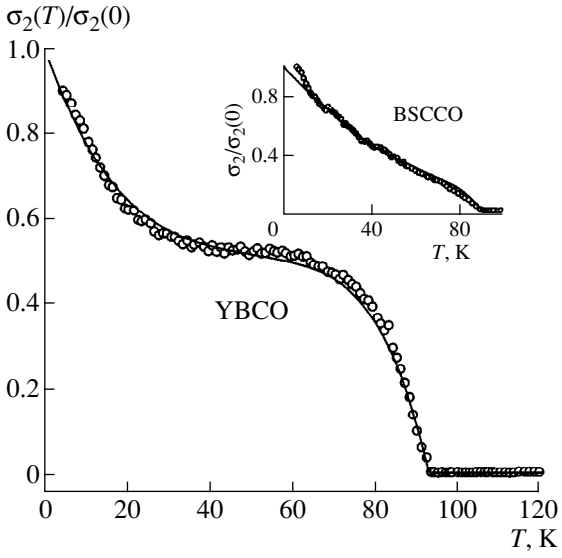

Fig. 13. Comparison between the calculated (solid line) and measured (circles) values of $\sigma_2(T)/\sigma_2(0)$ of the YBCO single crystal [8]. The inset shows the measured and calculated values with Eq. (20) used for the temperature dependences of $\sigma_2(T)/\sigma_2(0)$ of the BSCCO crystal shown in Fig. 1.

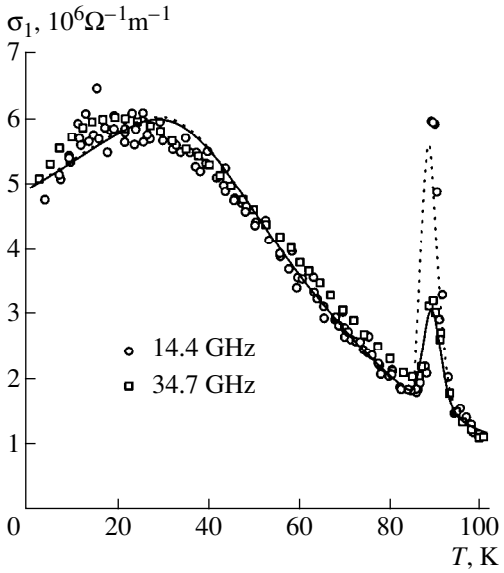

Fig. 14. Experimental data of $\sigma_1(T)$ at 14.4 and 34.7 GHz of the BSCCO single crystal [21] (symbols) and the calculations of $\sigma_1(T)$ (lines) using Eqs. (14), (21), and (6), with sample inhomogeneities taken into account ($\delta T_c = 2$ K).

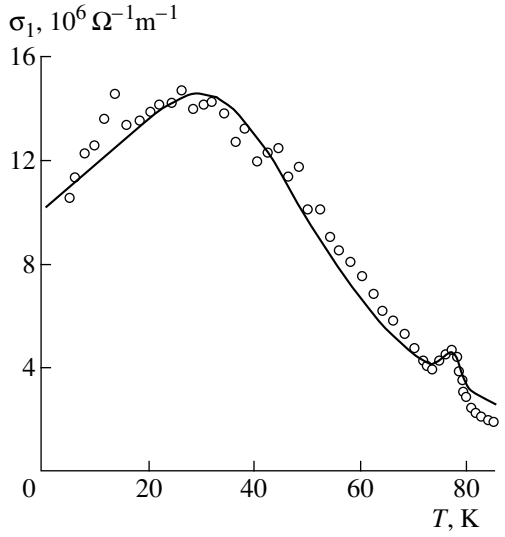

Fig. 15. Comparison of the experimental T-dependence of $\sigma_1(T)$ (open circles) of the TBCO single crystal at 24.8 GHz [23] with the one calculated using the modified two-fluid model (solid line) and taking the inhomogeneous broadening of the superconducting transition into account ($\delta T_c = 2.5$ K in Eq. (21)).

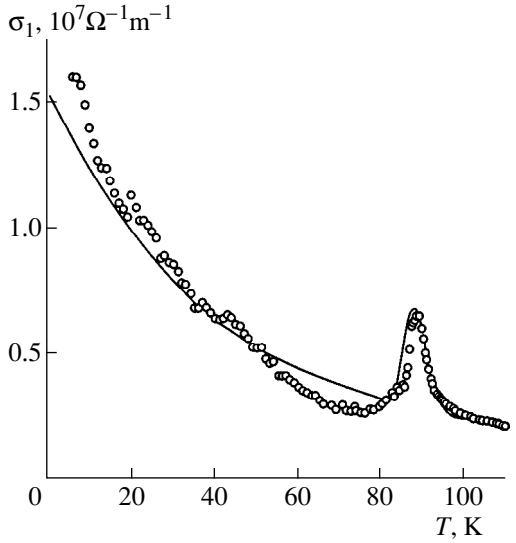

Fig. 16. The conductivity $\sigma_1(T)$ of the BSCCO single crystal at 9.4 GHz extracted from the surface impedance measurements of Fig. 1 and the calculation based on the modified two-fluid model, which takes the inhomogeneous broadening of the superconducting transition into account ($\delta T_c = 4.5$ K). $\sigma_1(T)$ does not have a broad peak at low temperatures in this particular case.

the magnetic field penetration depth (microscopic-scale disorder), the distribution of the microwave currents over the sample is uniform and the calculation of the effective impedance Z_{eff} of the sample reduces to two operations: adding the impedances Z_s of all regions in the specimen (with different T_c) that are connected in series along a current path and averaging over the sample volume. As the result, we obtain

$$Z_s^{\text{eff}}(T) = R_s^{\text{eff}}(T) + iX_s^{\text{eff}}(T) = \int_{\delta T_c} Z_s(T, T_c) f(T_c) dT_c, \tag{21}$$

where the distribution function $f(T_c)$ is such that the fraction of the sample volume with critical temperatures in the range $T_c < T < T_c + dT_c$ equals $f(T_c)dT_c$. In the simplest case, $f(T_c)$ is a Gaussian function. In the experiments of [14], the width of the superconducting resistive transition was approximately 0.4 K, which we equate to the width of the Gaussian distribution $f(T_c)$. Using general relations (6) with the effective impedance components obtained from Eq. (21), we calculate $\sigma_1^{\text{eff}}(T)$ near T_c and plot it together with the experimental data for YBCO in Fig. 3. The overall agreement is good.

In the framework of the discussed approach, $\sigma_1^{\text{eff}}(T)$ displays a narrow peak at $T^* = T_c - \delta T_c$. It is easy to check that the relative peak amplitude is approximately equal to

$$\frac{\sigma_1(T^*) - \sigma(T_c)}{\sigma(T_c)} \approx \begin{cases} \gamma & \text{if } \gamma > 1 \\ \gamma^2 & \text{if } \gamma < 0.1, \end{cases} \tag{22}$$

where $\gamma = \delta T_c/[T_c \omega \tau(T_c)]$, implying that the peak decreases with the decrease of the superconducting resistive transition width. Usually, experiments yield $\gamma > 1$ (e.g., the data of [14] give $\gamma \approx 7$ at 1.14 GHz); therefore, the peak amplitude should be inversely proportional to the frequency.

In calculating the $\sigma_1(T)$ curves for other specimens, we also applied the above procedure to incorporate corrections caused by the inhomogeneous broadening of the superconducting transition. We adjusted the previous calculations of $R_s(T)$ (Figs. 7, 8, and 10) and $\sigma_2(T)$ (Figs. 10, 12, and the inset to Fig. 13) by substituting the resulting $Z_s^{\text{eff}}(T)$ into Eq. (6) for the conductivity σ_1. The resulting curves for BSCCO and TBCO are shown in Figs. 14–16.

4. DISCUSSION AND CONCLUSION

We have presented a summary of measurements of the surface impedance $Z_s(T) = R_s(T) + iX_s(T)$ of high-quality YBCO, BSCCO, TBCO, and TBCCO crystals in the superconducting and normal states (table). For

frequencies $\lesssim$10 GHz, the common features of all these materials are the linear temperature dependence of the surface resistance ($\Delta R_s(T) \propto T$) and that of the surface reactance ($\Delta X_s(T) \propto \Delta\lambda_{ab}(T) \propto T$) at temperatures $T \ll T_c$; their rapid growth as $T \longrightarrow T_c$; and their behavior in the normal state corresponding to a linear T-dependence of $\Delta\rho_{ab}(T)$, with $R_s(T) = X_s(T) = \sqrt{\omega\mu_0\rho(T)/2}$. There are differences between the T-dependence of $Z_s(T)$ in BSCCO, TBCCO, or TBCO single crystals with tetragonal lattices and in YBCO crystals with an orthorhombic lattice. The linear resistivity region extends to near $T_c/2$ for the tetragonal materials and terminates near or below $T < T_c/3$ for YBCO. At higher temperatures, $R_s(T)$ of YBCO has a broad peak. In addition, the $\lambda_{ab}(T)$ curves of some YBCO single crystals have unusual features in the intermediate temperature range.

We describe all of the above features of $Z_s(T)$ and $\sigma_s(T) = \sigma_1(T) - i\sigma_2(T) = i\omega\mu_0/Z_s^2(T)$ of high-quality HTSC crystals by generalizing the well-known GC two-fluid model as follows.

(i) We introduce a temperature dependence of the relaxation time of the quasiparticles in accordance with the Bloch–Grüneisen law. We find that the $R_s(T)$ curves in different HTSC crystals are well described using Eqs. (14) or (15) for $1/\tau(T)$. In the latter equation, there is only one fitting parameter, $\kappa = \Theta/T_c$, while the other parameter $\beta = \tau(T_c)/\tau(0) \ll 1$ can be estimated directly from the experimental data with the help of Eqs. (16) and (17). The absence of the broad peak of $R_s(T)$ in tetragonal HTSC single crystals is due to a less rapid increase of $\tau(T)$ with decreasing the temperature. In other words, the value of β is smaller for YBCO crystals than for BSCCO, TBCO, or TBCCO. For the latter crystals, the residual losses $R_{\rm res}$ are usually large and they have to be taken into account.

(ii) We replace the well-known temperature dependence of the density of superconducting carriers in the GC model ($n_s = n(1 - t^4)$) by one of the functions in Eqs. (18), (19) or (20). All of these functions change linearly with temperature for $t \ll 1$ (see Eq. (1)). This permits one to extract the common and distinctive features of $X_s(T)$ and $\sigma_2(T)$ from different HTSC crystals.

It also follows from the equations of the modified two-fluid model that at low temperatures ($t \ll 1$) and low frequencies ($\omega\tau(0) < 1$), all curves of $Z_s(T)$ and $\sigma_s(T)$ have linear regions: $\sigma_1 \propto \alpha t/\beta$, since $n_n/n \approx \alpha t$ and $\tau \approx \tau(0) \approx \tau(T_c)/\beta$. Furthermore, $\Delta\sigma_2 \propto -\alpha t$. In accordance with Eq. (5), we then have $R_s \propto \alpha t/\beta$ and $\Delta X_s \propto \Delta\lambda \propto \alpha t/2$. As the temperature increases, the curve of $\sigma_1(t)$ passes through a maximum at $t \lesssim 0.5$ if the inequality (9) is valid. This peak is due to the superposition of two competing effects, namely, the decrease in the number of normal carriers as the temperature decreases (for $t < 1$) and the increase in the relaxation time (which saturates at $t \sim \beta^{1/5}$) where the impurity scattering starts to dominate. The features in the $X_s(T)$ and $\sigma_2(T)$ curves for YBCO single crystals in the intermediate temperature range (plateau [8] or bump [9]) can also be described within the framework of our modified two-fluid model if we take into account the modification of $n_s(t)$ described by Eq. (20) with $0 < \delta \le 0.5$. In HTSC single crystals, the narrow peak in the real part of the conductivity $\sigma_1(T)$ occurring near T_c can be explained in terms of an effective medium model, where the strong electron–phonon coupling of the quasiparticles and the inhomogeneous broadening of the superconducting transition are taken into account.

It is natural to compare the tenets of our phenomenological model with the results of microscopic theories. As was shown in [40] and [61], the simple formula (1), which defines the linear low-temperature dependence of the magnetic field penetration depth in the *ab*-plane of HTSC crystals, is consistent with the *d*-wave model [25–27] in the strong (unitary) scattering limit [31]. Besides, there is nothing foreign in introducing the function $1/\tau(T) \propto T^5$ for the purpose of characterizing scattering in the superconducting state of HTSC. A similar temperature dependence of the relaxation rate of quasiparticles follows from the SC model if the phonon corrections to the electromagnetic vertex are taken into account [94].

In the framework of our modified two-fluid model, the linear low-temperature dependence of the real part of the conductivity $\sigma_1(T)$ is consistent with a constant scattering rate, as it is in a normal metal. While the assumption of a Drude form of the conductivity is supported by the *d*-wave microscopic analysis [31], it was shown that in the usual impurity scattering models, pair correlations lead to a strong temperature dependence of the scattering time (neglecting vertex corrections), namely, $\tau(T) \propto T$ in the unitary limit or $\tau(T) \propto 1/T$ in the Born limit. An attempt to resolve this problem in [16] by choosing an intermediate scattering rate has not provided satisfactory results yet. Very recently, the authors of [95] and [96] argued that the experimental observation $\sigma_1(T) \propto T$ could be explained by the generalized Drude formula $\sigma_1(T) \propto n_{qp}(T)\tau(T)$ if the quasiparticle density varies as $n_{qp}(T) \propto T$ (as indeed happens for the *d*-wave pairing) and if the effective quasiparticle scattering time $\tau(T)$ saturates at low T. Various possible physical mechanisms of the temperature and energy dependence of τ are discussed in [95, 96]: scattering from the "holes" of the order parameter at impurity sites and scattering from extended defects. These mechanisms may provide the required saturation of $\tau(T)$ at low T. As was discussed recently in [97], the vertex corrections can also modify the low-temperature conductivity. However, the temperature dependence has not been investigated yet.

Nevertheless, the microscopic models aimed at investigating the microwave response using a pure d-wave order parameter symmetry cannot account for the linear section of the $R_s(T)$ curves extending to $T_c/2$ (at the frequencies 10 GHz and below) in tetragonal HTSC

single crystals, for the observation of radically different values of the slopes of $\sigma_2(T)$ for $T \ll T_c$ (corresponding to $\alpha > 1$ in Eq. (20)) observed on YBCO crystals [8–12], and for unusual features of $\sigma_2(T)$ in the intermediate temperatures range.

Recently, observations of unusual microwave properties of HTSC materials have caught the attention of a number of researchers [43–47, 55, 56]. These observations are tentatively attributed to the mixed ($d + s$) wave symmetry of the order parameter. Most studies deal with the low-temperature variation of the London penetration depth and its relation to an order parameter of mixed symmetry. In particular, it was shown in [55] that the low-temperature properties of $\lambda(T)$ can be used to distinguish between a pure *d*-wave order parameter and one with the ($s + id$) symmetry, having a small subdominant *s*-wave contribution in systems connected with a tetragonal lattice. Moreover, additions of impurities suppress the *d*-wave symmetric part to the benefit of the *s*-wave part. As a result, a variety of low-temperature dependences of $\lambda(T)$ can occur for various impurity concentrations. This allows one, in principle, to determine whether the order parameter of a superconductor with an orthorhombic lattice pertains to the ($s + id$) or the ($s + d$) symmetry [53]. In [46], the ($d + s$) model was generalized by taking the normal state anisotropy into account. This is the realistic approach to high-T_c cuprates with an orthorhombic distortion, since recent microwave conductivity data suggest that a substantial part of the *ab*-anisotropy of $\lambda(T)$ is a normal state effect. It was shown that such an anisotropy affects not only the *ab*-anisotropy of the transport coefficients but also the density of states and other thermodynamic quantities. The possible temperature variation of the penetration depth $\lambda(T)$ was analyzed recently in [56] in the framework of the ($d + s$) model of hybrid pairing. The slope of $\Delta\lambda(T) \propto T$ for $T \ll T_c$ and its dependence on the Δ_s/Δ_d admixture in the gap function were analyzed quantitatively, with the impurity scattering taken into account. However, the quantitative comparison of the latter calculation with the experimental data has not been performed yet. More interesting discoveries in this field of research can be expected in the near future.

ACKNOWLEDGMENTS

We are greatly indebted to N. Bontemps, V.T. Dolgopolov, V.F. Gantmakher, A.A. Golubov, L.M. Fisher, E.G. Maksimov, and V.P. Mineev for many helpful discussions. H.J. Fink thanks D.A. Bonn for permission to use the original data points of [14] in our figures. The research of Yu.A. Nefyodov and M.R. Trunin was supported by the Russian Foundation for Basic Research (projects no. 00-02-17053 and 00-02-04021) and Scientific Council on Superconductivity (project 96060), and in part by the Program for Russian–Dutch Research Cooperation (NWO).

REFERENCES

1. W. N. Hardy, D. A. Bonn, D. C. Morgan, *et al.*, Phys. Rev. Lett. **70**, 3999 (1993).
2. D. Achkir, M. Poirier, D. A. Bonn, *et al.*, Phys. Rev. B **48**, 13184 (1993).
3. S. Kamal, D. A. Bonn, N. Goldenfeld, *et al.*, Phys. Rev. Lett. **73**, 1845 (1994).
4. D. A. Bonn, S. Kamal, K. Zhang, *et al.*, Phys. Rev. B **50**, 4051 (1994).
5. J. Mao, D. H. Wu, J. L. Peng, *et al.*, Phys. Rev. B **51**, 3316 (1995).
6. D. A. Bonn, S. Kamal, K. Zhang, *et al.*, J. Phys. Chem. Solids **56**, 1941 (1995).
7. T. Jacobs, S. Sridhar, C. T. Rieck, *et al.*, J. Phys. Chem. Solids **56**, 1945 (1995).
8. M. R. Trunin, A. A. Zhukov, G. A. Emel'chenko, *et al.*, Pis'ma Zh. Éksp. Teor. Fiz. **65**, 893 (1997) [JETP Lett. **65**, 938 (1997)].
9. H. Srikanth, B. A. Willemsen, T. Jacobs, *et al.*, Phys. Rev. B **55**, R14733 (1997).
10. A. A. Zhukov, M. R. Trunin, A. T. Sokolov, *et al.*, Zh. Éksp. Teor. Fiz. **112**, 2210 (1997) [JETP **85**, 1211 (1997)].
11. H. Srikanth, Z. Zhai, S. Sridhar, *et al.*, Phys. Rev. B **57**, 7986 (1998).
12. M. R. Trunin, A. A. Zhukov, and A. T. Sokolov, J. Phys. Chem. Solids **59**, 2125 (1998).
13. S. Kamal, R. Liang, A. Hosseini, *et al.*, Phys. Rev. B **58**, R8933 (1998).
14. A. Hosseini, R. Harris, S. Kamal, *et al.*, Phys. Rev. B **60**, 1349 (1999).
15. L. A. de Vaulchier, J. P. Vieren, Y. Guldner, *et al.*, Europhys. Lett. **33**, 153 (1996).
16. S. Hensen, G. Müller, C. T. Rieck, *et al.*, Phys. Rev. B **56**, 6237 (1997).
17. S. Djordjevich, L. A. de Vaulchier, N. Bontemps, *et al.*, Eur. Phys. J. B **5**, 847 (1998).
18. E. Farber, G. Deutscher, J. P. Contour, *et al.*, Eur. Phys. J. B **5**, 159 (1998).
19. T. Jacobs, S. Sridhar, Q. Li, *et al.*, Phys. Rev. Lett. **75**, 4516 (1995).
20. T. Shibauchi, N. Katase, T. Tamegai, *et al.*, Physica C (Amsterdam) **264**, 227 (1996).
21. S.-F. Lee, D. C. Morgan, R. J. Ormeno, *et al.*, Phys. Rev. Lett. **77**, 735 (1996).
22. D. V. Shovkun, M. R. Trunin, A. A. Zhukov, *et al.*, Pis'ma Zh. Éksp. Teor. Fiz. **71**, 132 (2000) [JETP Lett. **71**, 92 (2000)].
23. D. M. Broun, D. C. Morgan, R. J. Ormeno, *et al.*, Phys. Rev. B **56**, R11443 (1997).
24. J. R. Waldram, D. M. Broun, D. C. Morgan, *et al.*, Phys. Rev. B **59**, 1528 (1999).
25. A. Millis, H. Monien, and D. Pines, Phys. Rev. B **42**, 167 (1990).

26. H. Monien, P. Monthoux, and D. Pines, Phys. Rev. B **43**, 275 (1991).
27. P. Monthoux, A. Balatsky, and D. Pines, Phys. Rev. B **46**, 14803 (1992).
28. P. J. Hirschfeld and N. Goldenfeld, Phys. Rev. B **48**, 4219 (1993).
29. J. P. Carbotte and C. Jiang, Phys. Rev. B **48**, 4231 (1993).
30. H. Won and K. Maki, Phys. Rev. B **49**, 1397 (1994).
31. P. J. Hirschfeld, W. O. Putikka, and D. J. Scalapino, Phys. Rev. Lett. **71**, 3705 (1993); Phys. Rev. B **50**, 4051 (1994).
32. D. J. Scalapino, Phys. Rep. **250**, 329 (1995).
33. J. Annett, N. Goldenfeld, and A. Leggett, in *Physical Properties of High Temperature Superconductors V*, Ed. by D. M. Ginsberg (World Scientific, Singapore, 1996).
34. K. Maki and H. Won, J. Phys. I **6**, 2317 (1996).
35. Yu. A. Izyumov, Usp. Fiz. Nauk **167**, 465 (1997) [Phys. Usp. **40**, 445 (1997)]; Usp. Fiz. Nauk **169**, 225 (1999).
36. R. A. Klemm and S. H. Liu, Phys. Rev. Lett. **74**, 2343 (1995).
37. V. Z. Kresin and S. A. Wolf, Phys. Rev. B **41**, 4278 (1990); **46**, 6458 (1992); **51**, 1229 (1995).
38. A. A. Golubov, M. R. Trunin, A. A. Zhukov, *et al.*, Pis'ma Zh. Éksp. Teor. Fiz. **62**, 477 (1995) [JETP Lett. **62**, 496 (1995)].
39. S. D. Adrian, M. E. Reeves, S. A. Wolf, *et al.*, Phys. Rev. B **51**, 6800 (1995).
40. M. R. Trunin, Usp. Fiz. Nauk **168**, 931 (1998) [Phys. Usp. **41**, 843 (1998)].
41. N. Klein, N. Tellmann, H. Schulz, *et al.*, Phys. Rev. Lett. **71**, 3355 (1993).
42. Q. P. Li, E. C. Koltenbah, and R. Joynt, Phys. Rev. B **48**, 437 (1993).
43. R. Combescot and X. Leyronas, Phys. Rev. Lett. **75**, 3732 (1995).
44. C. O'Donovan and J. P. Carbotte, Phys. Rev. B **52**, 4568 (1995); Phys. Rev. B 55, 8520 (1997).
45. H. Kim and E. J. Nicol, Phys. Rev. B **52**, 13576 (1995).
46. M. T. Beal-Monod and K. Maki, Phys. Rev. B **55**, 11730 (1997); Phys. Rev. B **53**, 5775 (1996); Phys. Rev. B **55**, 1194 (1997).
47. S. V. Pokrovsky and V. L. Pokrovsky, Phys. Rev. B **54**, 13275 (1996).
48. K. A. Musaelian, J. Betouras, A. V. Chubukov, *et al.*, Phys. Rev. B **53**, 3598 (1996).
49. Y. Ren, J. Xu, and C. S. Ting, Phys. Rev. B **53**, 2249 (1996).
50. A. A. Shapoval, Pis'ma Zh. Éksp. Teor. Fiz. **64**, 570 (1996) [JETP Lett. **64**, 625 (1996)].
51. M. Liu, D. Y. Xing, and Z. D. Wang, Phys. Rev. B **55**, 3181 (1997).
52. E. A. Pashitskiĭ and V. I. Pentegov, Zh. Éksp. Teor. Fiz. **111**, 298 (1997) [JETP **84**, 164 (1997)].
53. M. T. Beal-Monod, Phys. Rev. B **58**, 8830 (1998); Physica C (Amsterdam) **298**, 59 (1998).
54. I. Schürrer, E. Schachinger, and J. P. Carbotte, Physica C (Amsterdam) **303**, 287 (1998).
55. R. Modre, I. Schürrer, and E. Schachinger, Phys. Rev. B **57**, 5496 (1998).
56. Yu. A. Nefyodov, A. A. Golubov, M. R. Trunin, *et al.*, Physica B (Amsterdam) **284** (2000) (in press).
57. D. A. Bonn, P. Dosanjh, R. Liang, *et al.*, Phys. Rev. Lett. **68**, 2390 (1992).
58. K. Zhang, D. A. Bonn, R. Liang, *et al.*, Appl. Phys. Lett. **62**, 3019 (1993).
59. D. A. Bonn, R. Liang, T. M. Riseman, *et al.*, Phys. Rev. B **47**, 11314 (1993).
60. H. Kitano, T. Shibauchi, K. Uchinokura, *et al.*, Phys. Rev. B **51**, 1401 (1995).
61. M. R. Trunin, J. Supercond. **11**, 381 (1998).
62. S. M. Quinlan, D. J. Scalapino, and N. Bulut, Phys. Rev. B **49**, 1470 (1994).
63. G. M. Eliashberg, Zh. Éksp. Teor. Fiz. **38**, 966 (1960) [Sov. Phys. JETP **11**, 696 (1960)]; Pis'ma Zh. Éksp. Teor. Fiz. **48**, 275 (1988) [JETP Lett. **48**, 305 (1988)].
64. W. E. Pickett, J. Supercond. **4**, 397 (1991).
65. V. L. Ginzburg and E. G. Maksimov, Sverkhprovodimost': Fiz., Khim., Tekh. **5**, 1543 (1992).
66. A. A. Golubov, M. R. Trunin, A. A. Zhukov, *et al.*, J. Phys. I **6**, 2275 (1996).
67. A. Bille and K. Scharnberg, J. Phys. Chem. Solids **59**, 2110 (1998).
68. C. M. Varma, P. B. Littlewood, S. Schmitt-Rink, *et al.*, Phys. Rev. Lett. **63**, 1996 (1989).
69. E. Abrahams, J. Phys. I **6**, 2191 (1996).
70. P. W. Anderson, Physica C (Amsterdam) **185–189**, 11 (1991).
71. P. W. Anderson, *Theory of Superconductivity in the High-T_c Cuprates* (Princeton Univ. Press, Princeton, 1997).
72. P. A. Lee, Phys. Rev. Lett. **71**, 1887 (1993).
73. M. R. Trunin, A. A. Zhukov, G. E. Tsydynzhapov, *et al.*, Pis'ma Zh. Éksp. Teor. Fiz. **64**, 783 (1996) [JETP Lett. **64**, 832 (1996)].
74. H. J. Fink, Phys. Rev. B **58**, 9415 (1998); **61**, 6346 (2000).
75. H. J. Fink and M. R. Trunin, Physica B (Amsterdam) **284**, 923 (2000).
76. C. S. Gorter and H. Casimir, Phys. Z. **35**, 963 (1934).
77. N. E. Glass and W. F. Hall, Phys. Rev. B **44**, 4495 (1991).
78. H. K. Olsson and R. H. Koch, Phys. Rev. Lett. **68**, 2406 (1992).
79. A. A. Golubov, M. R. Trunin, S. V. Shulga, *et al.*, Physica C (Amsterdam) **213**, 139 (1993).
80. M. L. Horbach, W. van Saarlos, and D. A. Huse, Phys. Rev. Lett. **67**, 3464 (1991).

81. S. M. Anlage, J. Mao, J. C. Booth, *et al.*, Phys. Rev. B **53**, 2792 (1996).

82. G. M. Eliashberg, Zh. Éksp. Teor. Fiz. **39**, 1437 (1960) [Sov. Phys. JETP **12**, 1000 (1961)].

83. A. E. Karakozov, E. G. Maksimov, and S. A. Mashkov, Zh. Éksp. Teor. Fiz. **68**, 1937 (1975) [Sov. Phys. JETP **41**, 971 (1975)].

84. F. Marsiglio, Phys. Rev. B **44**, 5373 (1991).

85. A. E. Karakozov, E. G. Maksimov, and A. A. Mikhaĭlovskiĭ, Zh. Éksp. Teor. Fiz. **102**, 132 (1992) [Sov. Phys. JETP **75**, 70 (1992)].

86. O. V. Dolgov, E. G. Maksimov, A. E. Karakozov, *et al.*, Solid State Commun. **89**, 827 (1994).

87. G. V. Klimovich, A. V. Rylyakov, and G. M. Eliashberg, Pis'ma Zh. Éksp. Teor. Fiz. **53**, 381 (1991) [JETP Lett. **53**, 399 (1991)].

88. A. A. Mikhailovsky, S.V. Shulga, A. E. Karakozov, *et al.*, Solid State Commun. **80**, 511 (1991).

89. R. T. Collins, Z. Schlesinger, F. Holtzberg, *et al.*, Phys. Rev. B **43**, 8701 (1991).

90. J. Rammer, Europhys. Lett. **5**, 77 (1988).

91. A. Andreone, C. Cantoni, A. Cassinese, *et al.*, Phys. Rev. B **56**, 7874 (1997).

92. E. G. Maksimov, D. Yu. Savrasov, and S. Yu. Savrasov, Usp. Fiz. Nauk **167**, 354 (1997).

93. M. R. Trunin, A. A. Zhukov, and A. T. Sokolov, Zh. Éksp. Teor. Fiz. **111**, 696 (1997) [JETP **84**, 383 (1997)].

94. G. M. Eliashberg, G. V. Klimovich, and A. V. Rylyakov, J. Supercond. **4**, 393 (1991).

95. M. H. Hettler and P. J. Hirschfeld, Phys. Rev. B **61**, 11313 (2000).

96. A. J. Berlinsky, D. A. Bonn, R. Harris, *et al.*, Phys. Rev. B **61**, 9088 (2000).

97. A. C. Durst and P. A. Lee, cond-mat/9908182.